processes

MDPI

Article

Enhancing Accuracy in Numerical Simulations for High-Speed Flows: Integrating High-Order Corrections with Weighted Essentially Non-Oscillatory Flux

Yonghua Yan [1], Yong Yang [2,*], Shiming Yuan [1] and Caixia Chen [3]

[1] Department of Mathematics and Statistical Sciences, Jackson State University, Jackson, MS 39217, USA; yonghua.yan@jsums.edu (Y.Y.); shiming.yuan@students.jsums.edu (S.Y.)
[2] Department of Mathematics, West Texas A&M University, Canyon, TX 79016, USA
[3] Department of Mathematics and Computer Science, Tougaloo College, Tougaloo, MS 39174, USA; cchen1@tougaloo.edu
* Correspondence: yyang@wtamu.edu

Abstract: This study introduces a novel method to enhance numerical simulation accuracy for high-speed flows by refining the weighted essentially non-oscillatory (WENO) flux with higher-order corrections like the modified weighted compact scheme (MWCS). Numerical experiments demonstrate improved sharpness in capturing shock waves and stability in complex conditions like two interacting blast waves. Key highlights include simultaneous capture of small-scale smooth fluctuations and shock waves with precision surpassing the original WENO and MWCS methods. Despite the significantly improved accuracy, the extra computational cost brought by the new method is only marginally increased compared to the original WENO, and it outperforms MWCS in both accuracy and efficiency. Overall, this method enhances simulation fidelity and effectively balances accuracy and computational efficiency across various problems.

Keywords: numerical scheme; WENO; MWCS

Citation: Yan, Y.; Yang, Y.; Yuan, S.; Chen, C. Enhancing Accuracy in Numerical Simulations for High-Speed Flows: Integrating High-Order Corrections with Weighted Essentially Non-Oscillatory Flux. *Processes* **2024**, *12*, 642. https://doi.org/10.3390/pr12040642

Academic Editor: Ireneusz Zbicinski

Received: 16 February 2024
Revised: 14 March 2024
Accepted: 21 March 2024
Published: 24 March 2024

1. Introduction

High-order numerical schemes are essential tools in the realm of computational fluid dynamics, enabling the accurate simulation of the complex physical phenomena encountered in diverse scientific and engineering applications. Over the past two decades, significant progress has been made in the development of high-order schemes including but not limited to compact difference schemes [1–3], essentially non-oscillatory (ENO) schemes [4–6] and their weighted counterparts (WENO) [7–9], discontinuous Galerkin (DG) methods [10–12], spectral element (SE) methods [13], spectral volume methods (SVM) [14,15], spectral difference methods (SDM) [16,17], group velocity control schemes [18], and hybrid schemes [19,20]. These schemes offer sophisticated techniques for discretizing partial differential equations, facilitating the precise representation of intricate flow dynamics, wave propagation, and other phenomena characterized by sharp gradients and discontinuities. ENO schemes represent a significant advancement in high-order numerical techniques and are renowned for their robustness and ability to mitigate spurious oscillations near discontinuities. By employing sophisticated stencil selection procedures and weighted reconstructions, ENO schemes achieve high-order accuracy while maintaining stability in the presence of shock waves and other discontinuities. DG methods have garnered considerable attention in recent years as a versatile framework for high-order discretization of partial differential equations. DG methods partition the computational domain into disjoint elements and employ polynomial approximations within each element, facilitating accurate representation of solution gradients and discontinuities. By introducing discontinuities at element interfaces and employing suitable numerical fluxes, DG methods effectively handle shocks and

other complex flow phenomena, making them well-suited for a wide range of applications, including compressible flows, turbulence modeling, and multi-phase flow simulations. SE methods represent yet another class of high-order numerical techniques, leveraging the spectral accuracy of polynomial approximations within each element to achieve exceptionally high levels of solution accuracy. By combining the advantages of spectral accuracy with the flexibility of element-based discretization, SE methods offer a robust framework for simulating complex flow phenomena with superior accuracy and efficiency. These methods have found widespread applications in turbulent flow simulations, aerodynamics, and environmental fluid dynamics, among others. SVM and SDM also belong to the family of spectral-based numerical techniques, offering alternative approaches for high-order discretization of partial differential equations. SVMs integrate the advantages of spectral accuracy with the concept of control volumes, allowing for accurate representation of fluxes and gradients within each computational cell. SDMs, on the other hand, combine spectral approximations with finite difference formulations, offering a balance between accuracy and computational efficiency. Both SVMs and SDMs have demonstrated effectiveness in simulating a wide range of flow phenomena, including turbulent flows, shock waves, and combustion processes. Group velocity control schemes represent a unique approach to high-order numerical discretization, focusing on controlling the propagation characteristics of numerical schemes to enhance stability and accuracy. By manipulating the group velocity of numerical methods through suitable modifications to the discretization scheme, these methods mitigate dispersion and dissipation errors, leading to improved fidelity in wave propagation simulations. Group velocity control schemes have found applications in a diverse range of fields, including acoustics, electromagnetics, and solid mechanics. Hybrid schemes represent a synthesis of multiple numerical methodologies, leveraging the strengths of different approaches to achieve optimal performance in diverse flow scenarios. By combining elements of finite volume, finite difference, and spectral methods, hybrid schemes offer a versatile framework for simulating complex flow phenomena with high accuracy and efficiency.

Among the plethora of high-order numerical schemes available, weighted essentially non-oscillatory (WENO) schemes and compact schemes have emerged as leading contenders due to their ability to achieve exceptional accuracy and resolution. WENO schemes, conceptualized by Liu et al. in 1994 [7], have garnered widespread acclaim for their capacity to minimize numerical oscillations near discontinuities while maintaining high-order accuracy. The fundamental principle underlying WENO schemes lies in their weighted reconstruction approach, which combines multiple local polynomial reconstructions to generate a globally smooth and accurate approximation of the solution. This unique methodology has proven highly effective in capturing sharp gradients and discontinuities encountered in fluid dynamics, combustion, and other complex flow phenomena. Researchers have proposed several improved variants of WENO schemes to address specific challenges encountered in numerical simulations. These variants include WENO-JS [8], which implements a new smoothness indicator by utilizing the Lagrange form of interpolation polynomials. Additionally, modified versions such as WENO-Z [21] have been developed to reduce numerical dissipation near shocks while maintaining high-order accuracy with a global smoothness indicator that is recombined from all the stencils of WENO-JS. Building upon this, Castro et al. [22] developed a comprehensive framework for higher-order smoothness indicators, thereby enabling the extension of WENO-Z to achieve arbitrary odd-order precision. Ha et al. [23] contributed by designing a novel smoothness indicator, which, upon evaluation within the stencil, facilitated the creation of a fifth-order, accurate WENO-Z scheme specifically tailored for first-order critical points. Acker et al. [24] further advanced the field by introducing WENO-Z+, which enhances numerical resolution through the manipulation of less smooth sub-stencils. Wang et al. [25] uncovered a limitation in the accuracy of fifth-order WENO-Z schemes at high-order critical points. To address this issue, they proposed a remedy in the form of a new fifth-order scheme termed WENO-D. This approach incorporates a corrective function to adjust the

convergence accuracy relative to the weight function employed in the WENO-Z method. The central WENO (CWENO) [26,27] schemes prioritize the central stencil as the most stable, particularly emphasizing its importance in smooth flow conditions. In such scenarios, the method consistently gravitates towards the reliability of the central stencil. Conversely, in instances of non-smooth flow, the utilization of smoothness indicators enables the reconstruction process to identify and select the smoothest one-sided stencil available. The adaptive-order WENO (WENO-AO) scheme [28] uses a convex combination of fourth-degree polynomial and three quadratic polynomials to propose a new adaptive fifth-order scheme, and Legendre polynomials are used to calculate the smoothness indicators.

In contrast, compact schemes, pioneered by Lele in 1992 [1], are distinguished by their compact stencil and high-order accuracy. The compactness of these schemes refers to the fact that they require fewer grid points compared to traditional finite difference schemes of similar accuracy. These schemes excel in efficiently simulating smooth solutions with minimal numerical dispersion and dissipation. The crux of compact schemes lies in their finite difference approximations with compact stencils, which allow for the representation of higher-order spatial derivatives within a smaller computational domain. As a result, compact schemes have found widespread use in applications such as aerodynamics, acoustics, and other fields where accurately resolving smooth, high-frequency features is paramount. However, the implementation of compact schemes can be challenging due to the need for specialized techniques to handle boundary conditions and non-uniform grids effectively. A weighted compact scheme (WCS) introduced by Jiang, Shan, and Liu [29] employs the WENO weighting method to evaluate stencil candidates. WCS enhances accuracy by utilizing Hermite polynomials instead of Lagrange within each candidate. In shock regions, WCS effectively controls the contributions of different stencils to mitigate the impact of those containing shocks or discontinuities. Nevertheless, WCS, as originally formulated, exhibits limitations when applied to solving the Euler equations with shocks, as it does not sufficiently address global dependency issues associated with derivatives used in compact schemes. In response to these challenges, Fu et al. [30] proposed the modified weighted compact scheme (MWCS). This method combines elements of the WENO and WCS to address the shortcomings encountered in the approximation of fluxes on Euler equations. By the integration, MWCS aims to eliminate oscillations while facilitating the local computation of weight coefficients for pressure and density at each time step. However, MWCS incurs additional computational costs compared to the conventional WENO scheme due to the extra work in solving a tridiagonal system.

This paper proposes a method to enhance numerical simulation accuracy, especially for shock–turbulence interactions in which a shock propagates into a small-scale smooth flow. This method corrects the numerical flux obtained by WENO using the concept of WCS as inspired by the idea of MWCS and effectively mitigates the conventional trade-off between accuracy and computational efficiency. The structure of this paper is as follows: Section 2 introduces the numerical formulas utilized in the study. In Section 3, we present the numerical simulation results for three one-dimensional shock tube problems: Sod, Shu–Osher, and two interacting blast waves. Section 4 offers a comparison and discussion of the numerical results obtained using the original WENO, MWCS, and the WENO with flux correction. Finally, Section 5 summarizes the findings and provides concluding remarks.

2. Numerical Formula

This section outlines the numerical formulations of MWCS and a new approach to enhance accuracy by correcting the WENO flux using high-order WCS.

To comprehensively examine these schemes within a unified framework, we begin with the scalar conservation equation in the one-dimensional case (Equation (1)). This provides a convenient starting point for comparing and contrasting the various approaches.

$$\frac{\partial}{\partial t}u(x,t) + \frac{\partial}{\partial x}F(u(x,t)) = 0 \tag{1}$$

The spatial discretization utilizes the following grid configuration, which is also illustrated in Figure 1.

$$x_j \equiv \frac{1}{2}\left(x_{j-\frac{1}{2}} + x_{j+\frac{1}{2}}\right),\ h_j \equiv x_{j+\frac{1}{2}} - x_{j-\frac{1}{2}},\ j = 1, 2, \ldots, N. \tag{2}$$

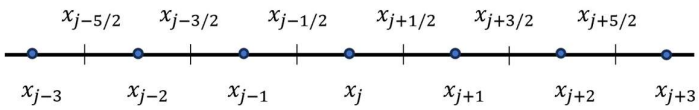

Figure 1. Grid configuration. The cell centers are represented by dots, and the cell interfaces are denoted by triangles.

The numerical flux $\hat{F}$ is associated with the original function F through an implicit definition represented by the following integral:

$$\hat{F}_j = \hat{F}\left(u(x_j,\ t)\right) \equiv \frac{1}{h_j}\int_{x_{j-\frac{1}{2}}}^{x_{j+\frac{1}{2}}} F(\xi)d\xi \tag{3}$$

Thus, the convection term in Equation (1) at x_j can be expressed as follows:

$$F'_j = \frac{\partial}{\partial x}F(x_j) = \frac{F_{j+\frac{1}{2}} - F_{j-\frac{1}{2}}}{h_j} \tag{4}$$

Now, we can define H as the primitive function of $F(\xi)$ and its function value at the cell interfaces can be calculated by the following:

$$H_{j+\frac{1}{2}} = H\left(x_{j+\frac{1}{2}}\right) = \int_{-\infty}^{x_{j+\frac{1}{2}}} F(\xi)d\xi = \sum_{i=-\infty}^{j}\int_{x_{i-\frac{1}{2}}}^{x_{i+\frac{1}{2}}} F(\xi)d\xi = \sum_{i=-\infty}^{j}\hat{F}_i h_i \tag{5}$$

It is important to emphasize that the derivative of the primitive function at the cell interfaces aligns precisely with the numerical flux:

$$H'_{j+\frac{1}{2}} = F_{j+\frac{1}{2}} \tag{6}$$

Substituting Equation (6) into Equation (4), yields the following:

$$F'_j = \frac{H'_{j+\frac{1}{2}} - H'_{j-\frac{1}{2}}}{h_j} \tag{7}$$

The above methodology was introduced by reference [4], and the only numerical approximation is associated with computation for H', with all other computations being exact.

2.1. The 5th-Order WENO Scheme

The fundamental concept behind the WENO scheme is to derive a high-order approximation for the numerical flux by employing a weighted average of multiple lower-order candidate approximations. The weights assigned to these candidates are determined based on the "smoothness" characteristics of the original function on each stencil. In the pursuit of a fifth-order WENO scheme, three second-order approximations of $F_{j+1/2}$ are derived from three distinct candidate stencils as follows:

$$E_0 = \left\{\hat{F}_{j-2}, \hat{F}_{j-1}, \hat{F}_j\right\}, E_1 = \left\{\hat{F}_{j-1}, \hat{F}_j, \hat{F}_{j+1}\right\}, E_2 = \left\{\hat{F}_j, \hat{F}_{j+1}, \hat{F}_{j+2}\right\} \tag{8}$$

Opting for the Lagrange polynomial to achieve a second-order approximation of $F_{j+1/2}$ within these stencils results in the following expression:

$$F_{j+\frac{1}{2}}^{(E_0)} \approx \frac{1}{3}\hat{F}_{j-2} - \frac{7}{6}\hat{F}_{j-1} + \frac{11}{6}\hat{F}_j \tag{9a}$$

$$F_{j+\frac{1}{2}}^{(E_1)} \approx -\frac{1}{6}\hat{F}_{j-1} + \frac{5}{6}\hat{F}_j + \frac{1}{3}\hat{F}_{j+1} \tag{9b}$$

$$F_{j+\frac{1}{2}}^{(E_2)} \approx \frac{1}{3}\hat{F}_j + \frac{5}{6}\hat{F}_{j+1} - \frac{1}{6}\hat{F}_{j+2} \tag{9c}$$

To compute the weighted average of the three lower-order approximations mentioned earlier, we need to employ the optimal weights based on the "smoothness" characteristics of the stencils:

$$F_{j+\frac{1}{2}} = \omega_0 F_{j+\frac{1}{2}}^{(E_0)} + \omega_1 F_{j+\frac{1}{2}}^{(E_1)} + \omega_2 F_{j+\frac{1}{2}}^{(E_2)} \tag{10}$$

where $\omega_i = \frac{\gamma_i}{\gamma_0+\gamma_1+\gamma_2}$, $\gamma_i = \frac{c_i}{(\varepsilon+IS_i)^2}$, and $c_0 = \frac{1}{10}$, $c_1 = \frac{3}{5}$, and $c_2 = \frac{3}{10}$. IS_i represents the smoothness indicators [8].

The WENO scheme stands out as a highly effective numerical approach. However, its performance tends to exhibit a slight diffusivity in small-scale smooth regions.

2.2. Modified Weighted Compact Scheme (MWCS)

The foundational concept of the weighted compact scheme (WCS) [29] revolves around forming a weighted average of two third-order and one fourth-order approximations of the numerical flux. In a manner akin to the WENO scheme, WCS establishes three candidate stencils as follows:

$$E_0 = \left\{H_{j-3/2}, H_{j-1/2}, H_{j+1/2}\right\}, E_1 = \left\{H_{j-1/2}, H_{j+1/2}, H_{j+3/2}\right\}, E_2 = \left\{H_{j+1/2}, H_{j+3/2}, H_{j+5/2}\right\} \tag{11}$$

The numerical flux approximations, $\hat{F}_{j+1/2} = H\prime_{j+1/2}$, are computed by applying a compact scheme on these three stencils:

$$E_0: \; 2H'_{j-\frac{1}{2}} + H'_{j+\frac{1}{2}} \approx \frac{1}{2h_j}\left(-H_{j-\frac{3}{2}} - 4H_{j-\frac{1}{2}} + 5H_{j+\frac{1}{2}}\right) \tag{12a}$$

$$E_1: \; H'_{j-\frac{1}{2}} + 4H'_{j+\frac{1}{2}} + H'_{j+\frac{3}{2}} \approx \frac{3}{h_j}\left(H_{j+\frac{3}{2}} - H_{j-\frac{1}{2}}\right) \tag{12b}$$

$$E_2: \; H'_{j+\frac{1}{2}} + 2H'_{j+\frac{3}{2}} \approx \frac{1}{2h_j}\left(-5H_{j+\frac{1}{2}} + 4H_{j+\frac{3}{2}} + H_{j+\frac{5}{2}}\right) \tag{12c}$$

Similar to the WENO scheme, computing the weighted average of the three lower-order approximations yields the following results:

$$\begin{aligned}(2\omega_0+\omega_1)H'_{j-\frac{1}{2}} \quad &+(\omega_0+4\omega_1+\omega_2)H'_{j+\frac{1}{2}} + (\omega_1+2\omega_2)H'_{j+\frac{3}{2}} \\ &= \tfrac{\omega_0}{2h_j}\left(-H_{j-\frac{3}{2}} - 4H_{j-\frac{1}{2}} + 5H_{j+\frac{1}{2}}\right) + \tfrac{3\omega_1}{h_j}\left(H_{j+\frac{3}{2}} - H_{j-\frac{1}{2}}\right) \\ &+\tfrac{\omega_2}{2h_j}\left(-5H_{j+\frac{1}{2}} + 4H_{j+\frac{3}{2}} + H_{j+\frac{5}{2}}\right)\end{aligned} \tag{13}$$

where $\omega_i = \frac{\gamma_i}{\gamma_0+\gamma_1+\gamma_2}$, $\gamma_i = \frac{c_i}{\varepsilon+IS_i}$, and $c_0 = \frac{1}{18}$, $c_1 = \frac{8}{9}$, and $c_2 = \frac{1}{18}$.

After solving the tridiagonal linear system from Equation (13), the convection term can be calculated by Equation (7).

To resolve the instability issue of WCS in solving problems with strong discontinuity (sharp shock waves), the modified weighted compact scheme (MWCS) [30] integrates both WENO and WCS as follows:

$$\hat{F}_{j-1/2}^{(MWCS)} = (1-\alpha_j)\hat{F}_{j-1/2}^{(WCS)} + \alpha_j \hat{F}_{j-1/2}^{(WENO)} \tag{14}$$

where $\alpha = 1 - 0.5 * \left(1 - \frac{(IS_0 - IS_1)^2 + (IS_1 - IS_2)^2 + (IS_2 - IS_0)^2}{2 * \left(IS_0^2 + IS_1^2 + IS_2^2\right)}\right)$.

MWCS is capable of capturing both small-scale smooth flow and sharp shocks. However, this improvement comes with a significantly increased computational workload due to the extra work in solving the tridiagonal linear system.

2.3. WENO with Flux Correction

Inspired by the above two schemes, we propose a new method to enhance the accuracy of numerical simulations by correcting the WENO flux through the concept of WCS. The fundamental concept of this method is to amplify the weight of the central stencil E_1 under conditions of small-scale smooth flow.

Substituting Equations (5) and (6) in Equation (12b) yields the correction formula as follows:

$$F_{j+\frac{1}{2}} = \frac{3\hat{F}_{j+1} + 3\hat{F}_j - F_{j-\frac{1}{2}} - F_{j+\frac{3}{2}}}{4} \tag{15}$$

where $\hat{F}_{j+1}$ and $\hat{F}_j$ are the numerical flux at the cell centers, while $F_{j-\frac{1}{2}}$ and $F_{j+\frac{3}{2}}$ are the flux at the cell interfaces calculated by the WENO scheme. The corrections are exclusively applied to locations where the central stencil weight ω_1 of the WENO scheme falls below a predetermined threshold (set at 0.04 in this paper). The original WENO scheme achieves second-order accuracy within its stencils, whereas the WCS scheme achieves fourth-order accuracy within the central stencil. Through the flux correction at the central stencil, the newly devised method achieves fourth-order accuracy within the central stencil, thereby yielding a significant enhancement in overall accuracy. The algorithm can be succinctly summarized as follows:

- Step 1: Calculate all flux $F_{j+\frac{1}{2}}$ at the cell interfaces using Equation (10). Mark interfaces where ω_1 is smaller than the threshold;
- Step 2: Correct the flux $F_{j+\frac{1}{2}}$ using Equation (15) at the cell interfaces that have been marked in Step 1.

By incorporating this correction, the numerical simulation can effectively capture features of small-scale smooth flow with higher accuracy, all without imposing a significant increase in computational overhead. These enhancements will be thoroughly demonstrated and discussed in the upcoming sections.

3. Results

In this study, we validate and evaluate the proposed scheme through several benchmark tests of the one-dimensional Euler equation. These benchmark tests can reveal the ability of numerical schemes on resolving small scales (turbulence) and capturing strong discontinuities (shock waves). The one-dimensional Euler equation, expressed in vector and conservation form, is given as follows:

$$\frac{\partial}{\partial t}\begin{bmatrix}\rho\\ \rho u\\ E\end{bmatrix} + \frac{\partial}{\partial x}\begin{bmatrix}\rho u\\ \rho u^2 + p\\ u(E+p)\end{bmatrix} = 0 \tag{16}$$

where ρ, u, and E represent density, velocity, and total energy, respectively. p represents pressure and is calculated by $p = (\gamma - 1)\left(E - \frac{1}{2}\rho u^2\right)$.

3.1. Numerical Results Comparison against WENO and MWCS

The presented WENO with flux correction is applied to solve the one-dimensional Euler equations for three benchmark tests—the Sod shock tube problem, Shu–Osher problem, and two interacting blast waves problem. These problems serve as standard benchmarks in the evaluation of high-order schemes. Widely utilized in previous research, these test cases offer insight into the capability of numerical methods to handle turbulence and accurately

capture shock waves. Essentially, these scenarios present one-dimensional challenges representing high-speed flows with varied boundary treatments and initial conditions. The results are presented with a comparison against the ones of WENO and MWCS. Note that the exact solutions for the subsequent problems were obtained using WENO with fine grids, specifically with a grid number of $N = 1601$, and other results are simulated with coarse grids with $N = 201$.

3.1.1. Sod Shock Tube Problem

The Sod shock tube problem stands as a cornerstone in computational fluid dynamics (CFD) and gas dynamics, serving as a fundamental benchmark for evaluating the accuracy and robustness of numerical schemes. Introduced by Gary A. Sod in 1978 [31], this canonical problem presents a simple yet profound scenario that illuminates the intricate dynamics of shock wave propagation and fluid interactions within a compressible medium. In the Sod shock tube configuration, a long cylindrical tube is initially divided into two distinct regions by a thin diaphragm. One region contains high-pressure gas, while the other contains low-pressure gas, separated by the diaphragm. When the diaphragm is suddenly ruptured, a shock wave propagates into the low-pressure region, creating complex flow phenomena including rarefaction waves, contact discontinuities, and shock reflections. The significance of the Sod shock tube problem lies in its ability to encapsulate key aspects of compressible flow physics, making it an invaluable tool for validating numerical methods and assessing their performance in capturing shock wave dynamics, resolving discontinuities, and preserving solution accuracy.

To assess the shock-capturing capability of the proposed method, the Sod shock tube problem with the following initial conditions is conducted:

$$\begin{bmatrix} \rho_L \\ p_L \\ u_L \end{bmatrix} = \begin{bmatrix} 1.0 \\ 1.0 \\ 0.0 \end{bmatrix}, \begin{bmatrix} \rho_R \\ p_R \\ u_R \end{bmatrix} = \begin{bmatrix} 0.125 \\ 0.1 \\ 0.0 \end{bmatrix} \tag{17}$$

where the indices L and R denote conditions on the left- and right-hand sides, respectively, with the center located at $x = 0$.

Figure 2 illustrates the density profile in the Sod shock tube problem. Comparing WENO with flux correction to the original WENO and MWCS schemes, the WENO with flux correction exhibits a pronounced capability for capturing the shock with heightened precision. This augmentation enables the scheme to depict the shock phenomenon with sharper delineation and increased fidelity compared to its counterparts.

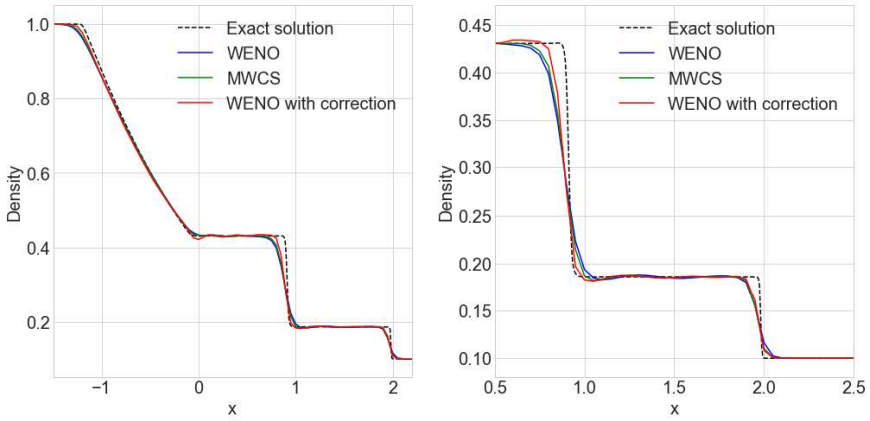

Figure 2. Density variation along the shock tube in Sod problem. (**a**) Global view; (**b**) enlarged perspective focused on the shock waves.

3.1.2. Shu–Osher Problem

The Shu–Osher problem, introduced by Chi-Wang Shu and Stanley Osher in 1989 [5], stands as a pivotal challenge in computational fluid dynamics (CFD) for evaluating numerical schemes in capturing complex shock wave interactions and resolving contact discontinuities. This problem involves the advection of a smooth scalar field over a sequence of periodic square waves, resulting in intricate shock wave dynamics and wave interactions. The significance of the Shu–Osher problem lies in its ability to test the robustness and accuracy of numerical methods, particularly in handling the challenge due to the sensitivity of entropy waves to numerical dissipation, which may lead to excessive damping.

To assess the efficacy of the proposed method in capturing shocks and their interaction with turbulence, the Shu–Osher problem is conducted. The same governing Equation (16) is solved, with the initial conditions specified as follows:

$$\begin{bmatrix} \rho_L \\ p_L \\ u_L \end{bmatrix} = \begin{bmatrix} 3.857143 \\ 10.33333 \\ 2.629369 \end{bmatrix}, \quad \begin{bmatrix} \rho_R \\ p_R \\ u_R \end{bmatrix} = \begin{bmatrix} 1 + 0.2\sin(5x) \\ 1.0 \\ 0.0 \end{bmatrix} \tag{18}$$

where the indices L and R denote conditions on the left and right-hand sides, respectively, with the center located at $x = 0$.

Figure 3 illustrates the density profile in the Shu–Osher shock tube problem. The outcomes derived from employing WENO with correction reveal its adeptness in sharply capturing small-scale smooth flow phenomena. In contrast, MWCS tends to blur the small-scale waves, while the original WENO scheme fares even worse, failing to adequately capture fluctuations altogether. This comparison underscores the superiority of WENO with correction in representing intricate flow dynamics, particularly at smaller scales. The precision of this approach contrasts starkly with the smearing effect observed with MWCS and the inability of the original WENO scheme to capture nuanced fluctuations.

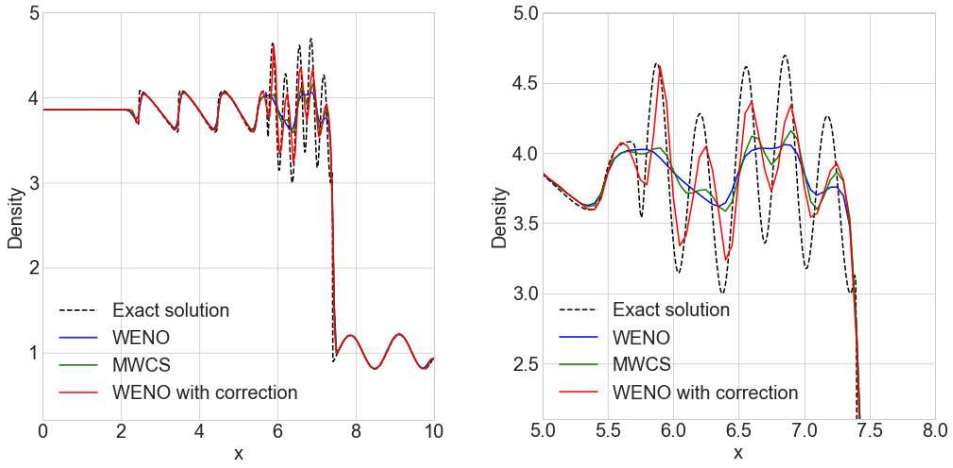

Figure 3. Density variation along the shock tube in the Shu–Osher problem. (**a**) Global view; (**b**) enlarged perspective focused on the small-scale smooth region.

3.1.3. Two Interacting Blast Waves Problem

The two interacting blast waves problem serves as a critical test case in CFD for studying shock wave interactions and the formation of complex flow patterns. Initially proposed as a benchmark by Woodward and Colella in 1984 [32], this scenario involves the collision of two shock waves traveling in opposite directions, resulting in intricate wave interactions and shock wave reflections. The significance of the two interacting blast waves problem lies in its relevance to various real-world phenomena, including explosion

dynamics, supersonic flow over obstacles, and astrophysical events such as supernova remnants. By simulating this problem, researchers can assess the capability of numerical methods to accurately capture shock wave dynamics, resolve contact discontinuities, and predict the formation of secondary shocks and rarefaction waves.

To assess the capability of the proposed method in simulating strong shock waves and multiple interactions, the two interacting blast waves problem is simulated with the initial conditions specified as follows:

$$\begin{bmatrix} \rho_L \\ p_L \\ u_L \end{bmatrix} = \begin{bmatrix} 1.0 \\ 1000.0 \\ 0.0 \end{bmatrix}, \quad \begin{bmatrix} \rho_M \\ p_M \\ u_M \end{bmatrix} = \begin{bmatrix} 1.0 \\ 0.01 \\ 0.0 \end{bmatrix}, \quad \begin{bmatrix} \rho_R \\ p_R \\ u_R \end{bmatrix} = \begin{bmatrix} 1.0 \\ 100.0 \\ 0.0 \end{bmatrix} \tag{19}$$

where the indices L, M, and R denote conditions in the left ($0 \leq x \leq 0.1$), middle ($0.1 < x \leq 0.9$), and right ($0.9 < x \leq 1.0$) regions, respectively.

Figure 4 illustrates the density profile in two interacting blast waves problem. The application of WENO with correction yields promising results in simulating the intricate interaction between two blast shock waves, surpassing the performance of both the original WENO and MWCS schemes. Notably, it demonstrates a superior capability in capturing shock phenomena with remarkable sharpness while also adeptly handling multiple interactions involving rarefactions and contact discontinuities. This development highlights the efficacy of WENO with correction in precisely depicting intricate flow dynamics, especially in situations characterized by interactions of shock waves.

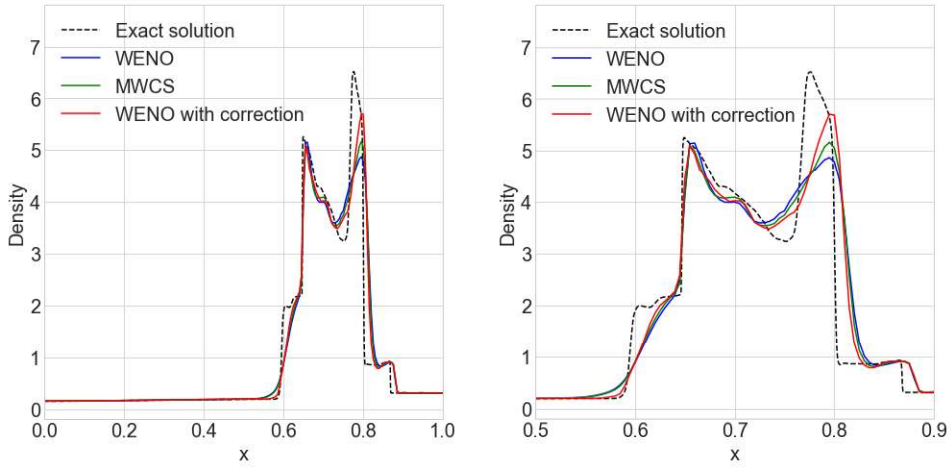

Figure 4. Density variation at $t = 0.038$ along the shock tube in two blast waves problem. (**a**) Global view; (**b**) enlarged perspective focused on the interaction of two blast waves.

3.2. Grid Convergence

Figure 5 illustrates the density distributions in Sod, Shu–Osher, and two blast waves problems, comparing the results obtained by the WENO with correction using a coarse grid ($N = 201$) and a fine grid ($N = 401$). Notably, the figure highlights the remarkable grid convergence exhibited by the WENO with correction, as evidenced by the alignment of results obtained from both grid resolutions. This convergence emphasizes the reliability and accuracy of the WENO scheme with correction across varying grid densities, thus bolstering confidence in its predictive capabilities for a wide range of fluid dynamics scenarios.

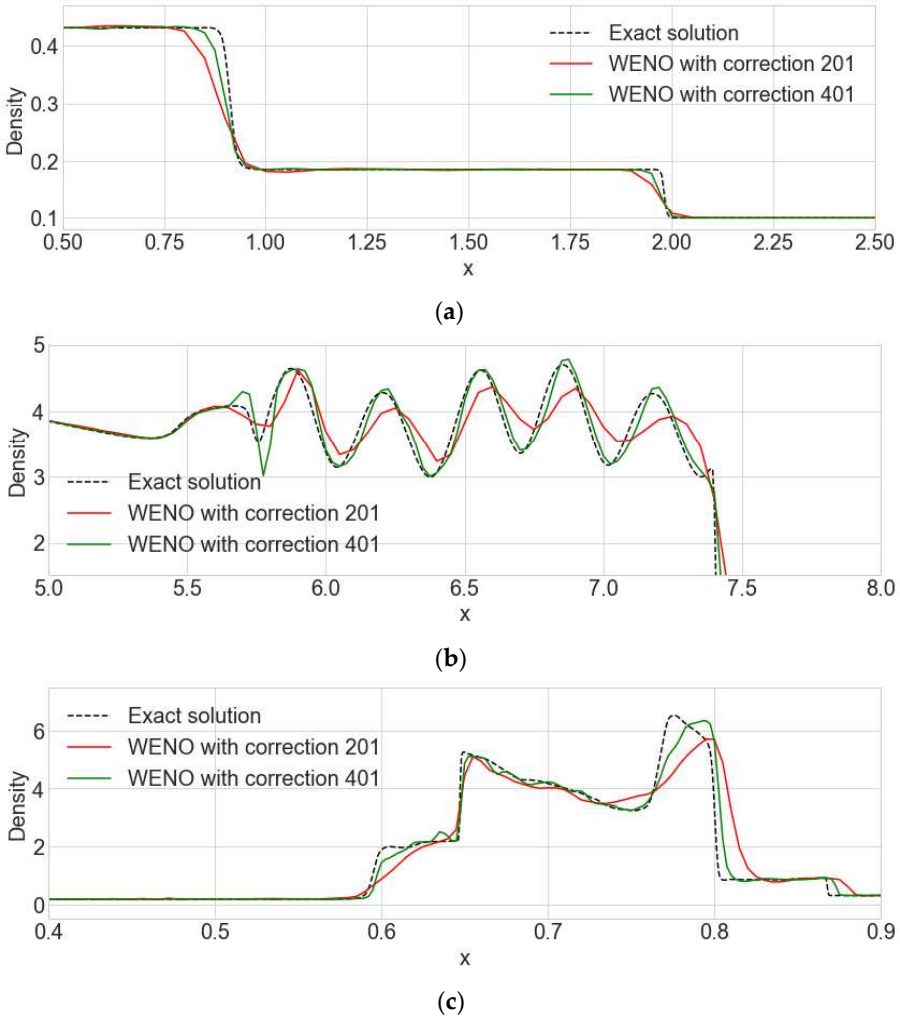

Figure 5. Density variation along the shock tube in the (**a**) Sod problem, (**b**) Shu–Osher problem, and (**c**) two interacting blast waves problem. Red lines represent the results using a coarse grid ($N = 201$), and green lines represent the results using a fine grid ($N = 401$).

3.3. Spatial Discretization Independence

Figure 6 demonstrates the consistency of numerical simulation outcomes when employing the Courant number for time step calculation versus using a fixed time step across three distinct shock tube problems. This coherence verifies the spatial discretization's independence from the time-marching approach.

3.4. Efficiency Comparison

Figure 7 presents a runtime comparison among the original WENO, the WENO with flux correction, and the MWCS schemes across three distinct shock tube problems. Each problem underwent three executions with each scheme, with the color bars representing the mean of the three results and the error bars depicting the standard deviations within this statistical analysis. Analysis of the figure reveals that while the WENO with flux correction exhibits slightly slower runtime compared to the original WENO, it showcases a substantial improvement over the MWCS scheme.

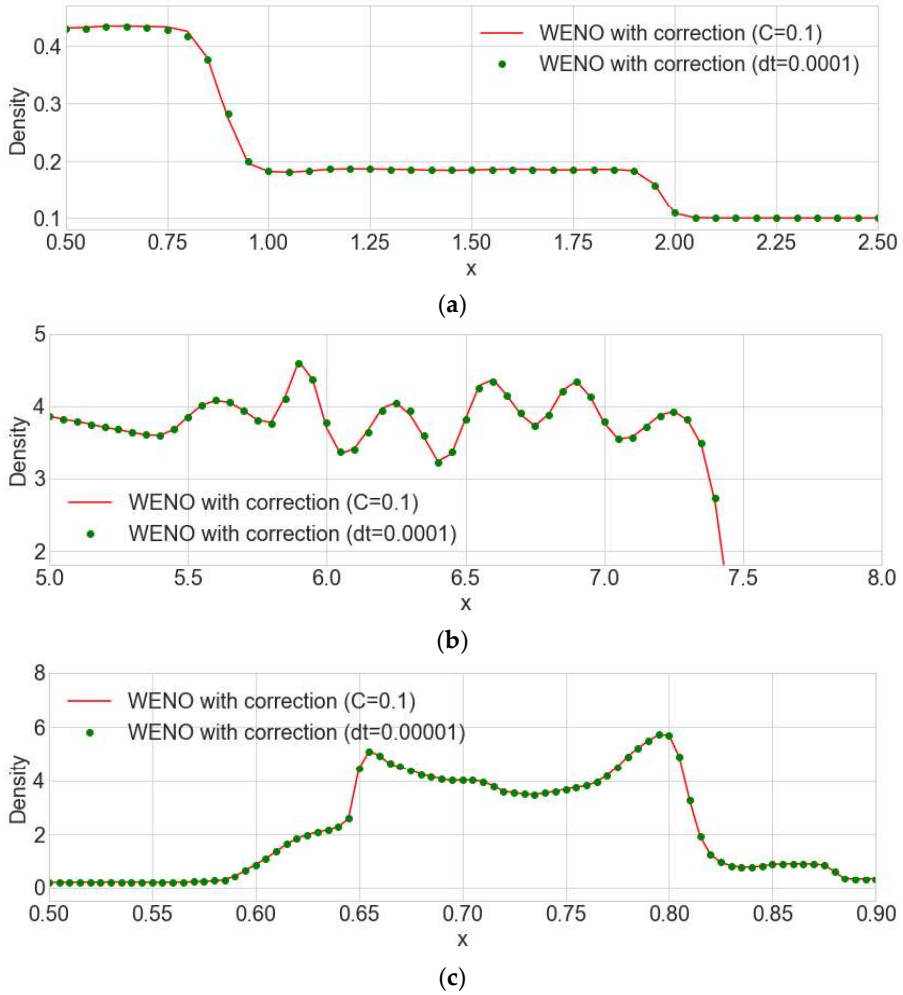

Figure 6. Density variation along the shock tube in the (**a**) Sod problem, (**b**) Shu–Osher problem, and (**c**) two interacting blast waves problem. Red lines represent the results using the Courant number $C = 0.1$, and green dots represent the results using fixed time step ($dt = 0.0001$ for the first two problems and $dt = 0.00001$ for the last problem).

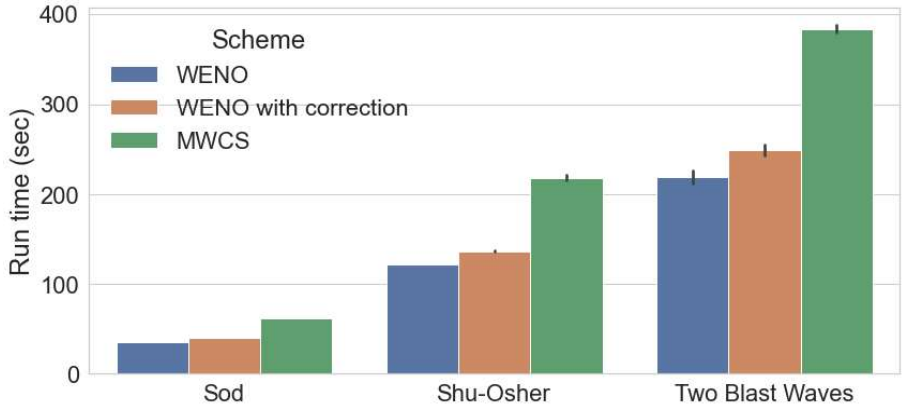

Figure 7. Run time comparison for different schemes. Each problem was executed three times with each scheme, and the rectangles display the average result. The error bars represent the standard deviations.

4. Discussion

According to the numerical experiments in the last section, the new method by correcting the WENO flux through the concept of WCS improves the ability to capture shock waves sharply and is stable when dealing with complex conditions such as two interacting blast waves. The grid convergence test also shows that this new method is grid independence. The consistency of numerical results of using the Courant number and fixed time step shows that this new method does not impose instability in time marching.

The highlights of this method are that it can capture small-scale smooth fluctuation and shock waves at the same time. Unlike the original WENO and MWCS that smeared the small-scale waves, this method captures the undulation in a more precise way. Another highlight is that while it improves the simulation accuracy significantly, its computing cost is just slightly increased compared to the original WENO, and it transcends the MWCS in both accuracy and computing cost.

The new method's applicability to any PDE model and its ability to increase accuracy at discontinuities hold significant implications for advancing numerical simulations across various domains. In fluid dynamics, structural mechanics, electromagnetics, and beyond, precise resolution of discontinuities promises more accurate predictions and optimizations in aerospace engineering, structural design, telecommunications, and electromagnetic compatibility analysis. The impact of this new method, while promising, remains open to further exploration and refinement, offering a potential pathway to more reliable simulations and deeper insights across scientific and engineering disciplines.

5. Conclusions

Building upon the ideas of MWCS, we have introduced a novel method aimed at enhancing the accuracy of numerical simulations by refining the WENO flux. This enhancement involves amplifying the influence of the central stencil under conditions of small-scale smooth flow. By integrating this correction, the numerical simulation becomes adept at capturing the nuances of small-scale smooth waves with heightened precision, all without imposing a significant increase in computational burden. This advancement enables the simulation to represent subtle variations and intricate dynamics inherent in the flow more accurately, thereby enhancing the overall fidelity of numerical simulations. Three one-dimensional benchmark cases of the Euler equation were conducted in this study for validation. In all the cases, the numerical solution given by the new method shows significant improvement in the capture of strong discontinuity and small-scale waves simultaneously. Grid convergence and spatial discretization independence were also conducted to confirm the accuracy of the results. In addition, an efficiency comparison was also made among the new method, original WENO, and MWCS, the results show that the new method only requires an acceptable amount of additional calculations compared to the original WENO and far less than what MWCS requires. This suggests that this new method effectively mitigates the conventional trade-off between accuracy and computational efficiency, presenting a promising avenue for advancing numerical simulations across diverse domains.

Author Contributions: Conceptualization and methodology, Y.Y. (Yong Yang) and Y.Y. (Yonghua Yan); formal analysis, Y.Y. (Yong Yang), Y.Y. (Yonghua Yan) and C.C.; writing—original draft preparation, Y.Y. (Yong Yang), Y.Y. (Yonghua Yan) and S.Y.; writing—review and editing, Y.Y. (Yong Yang), Y.Y. (Yonghua Yan) and C.C.; visualization, Y.Y. (Yong Yang), Y.Y. (Yonghua Yan) and S.Y. All authors have read and agreed to the published version of the manuscript.

Funding: This research is supported by the Mississippi NASA EPSCoR program.

Data Availability Statement: Data are contained within the article.

Conflicts of Interest: The authors declare no conflicts of interest.

References

1. Lele, S.K. Compact finite difference schemes with spectral-like resolution. *J. Comput. Phys.* **1992**, *103*, 16–42. [CrossRef]
2. Visbal, M.R.; Gaitonde, D.V. On the Use of Higher-Order Finite-Difference Schemes on Curvilinear and Deforming Meshes. *J. Comput. Phys.* **2002**, *181*, 155–185. [CrossRef]
3. Yee, H. Explicit and Implicit Multidimensional Compact High-Resolution Shock-Capturing Methods: Formulation. *J. Comput. Phys.* **1997**, *131*, 216–232. [CrossRef]
4. Shu, C.-W.; Osher, S. Efficient implementation of essentially non-oscillatory shock-capturing schemes. *J. Comput. Phys.* **1988**, *77*, 439–471. [CrossRef]
5. Shu, C.-W.; Osher, S. Efficient implementation of essentially non-oscillatory shock-capturing schemes, II. *J. Comput. Phys.* **1989**, *83*, 32–78. [CrossRef]
6. Harten, A.; Engquist, B.; Osher, S.; Chakravarthy, S.R. Uniformly High Order Accurate Essentially Non-oscillatory Schemes, III. *J. Comput. Phys.* **1997**, *131*, 3–47. [CrossRef]
7. Liu, X.-D.; Osher, S.; Chan, T. Weighted Essentially Non-oscillatory Schemes. *J. Comput. Phys.* **1994**, *115*, 200–212. [CrossRef]
8. Jiang, G.-S.; Shu, C.-W. Efficient Implementation of Weighted ENO Schemes. *J. Comput. Phys.* **1996**, *126*, 202–228. [CrossRef]
9. Shu, C.-W. High Order Weighted Essentially Nonoscillatory Schemes for Convection Dominated Problems. *SIAM Rev.* **2009**, *51*, 82–126. [CrossRef]
10. Cockburn, B.; Lin, S.-Y.; Shu, C.-W. TVB Runge-Kutta local projection discontinuous Galerkin finite element method for conservation laws III: One-dimensional systems. *J. Comput. Phys.* **1989**, *84*, 90–113. [CrossRef]
11. Cockburn, B.; Shu, C.-W. The Local Discontinuous Galerkin Method for Time-Dependent Convection-Diffusion Systems. *SIAM J. Numer. Anal.* **1998**, *35*, 2440–2463. [CrossRef]
12. Bassi, F.; Rebay, S. A High-Order Accurate Discontinuous Finite Element Method for the Numerical Solution of the Compressible Navier–Stokes Equations. *J. Comput. Phys.* **1997**, *131*, 267–279. [CrossRef]
13. Patera, A.T. A spectral element method for fluid dynamics: Laminar flow in a channel expansion. *J. Comput. Phys.* **1984**, *54*, 468–488. [CrossRef]
14. Wang, Z.; Huang, G.P. An Essentially Nonoscillatory High-Order Padé-Type (ENO-Padé) Scheme. *J. Comput. Phys.* **2002**, *177*, 37–58. [CrossRef]
15. Liu, Y.; Vinokur, M.; Wang, Z. Spectral (finite) volume method for conservation laws on unstructured grids V: Extension to three-dimensional systems. *J. Comput. Phys.* **2006**, *212*, 454–472. [CrossRef]
16. Liu, Y.; Vinokur, M.; Wang, Z. Spectral difference method for unstructured grids I: Basic formulation. *J. Comput. Phys.* **2006**, *216*, 780–801. [CrossRef]
17. Sun, Y.; Wang, Z.; Liu, Y. High-Order Multidomain Spectral Difference Method for the Navier-Stokes Equations. In Proceedings of the 44th AIAA Aerospace Sciences Meeting and Exhibit, Reno, NV, USA, 9–12 January 2006.
18. Ma, Y.; Fu, D. Fourth order accurate compact scheme with group velocity control (GVC). *Sci. China Math.* **2001**, *44*, 1197–1204. [CrossRef]
19. Wang, Z. Spectral (Finite) Volume Method for Conservation Laws on Unstructured Grids. Basic Formulation: Basic Formulation. *J. Comput. Phys.* **2002**, *178*, 210–251. [CrossRef]
20. Adams, N.; Shariff, K. A High-Resolution Hybrid Compact-ENO Scheme for Shock-Turbulence Interaction Problems. *J. Comput. Phys.* **1996**, *127*, 27–51. [CrossRef]
21. Borges, R.; Carmona, M.; Costa, B.; Don, W.S. An improved weighted essentially non-oscillatory scheme for hyperbolic conservation laws. *J. Comput. Phys.* **2008**, *227*, 3191–3211. [CrossRef]
22. Castro, M.; Costa, B.; Don, W.S. High order weighted essentially non-oscillatory WENO-Z schemes for hyperbolic conservation laws. *J. Comput. Phys.* **2011**, *230*, 1766–1792. [CrossRef]
23. Ha, Y.; Kim, C.H.; Lee, Y.J.; Yoon, J. An improved weighted essentially non-oscillatory scheme with a new smoothness indicator. *J. Comput. Phys.* **2013**, *232*, 68–86. [CrossRef]
24. Acker, F.; Borges, R.B.d.R.; Costa, B. An improved WENO-Z scheme. *J. Comput. Phys.* **2016**, *313*, 726–753. [CrossRef]
25. Wang, Y.; Wang, B.-S.; Don, W.S. Generalized Sensitivity Parameter Free Fifth Order WENO Finite Difference Scheme with Z-Type Weights. *J. Sci. Comput.* **2019**, *81*, 1329–1358. [CrossRef]
26. Levy, D.; Puppo, G.; Russo, G. Central WENO schemes for hyperbolic systems of conservation laws. *ESAIM Math. Model. Numer. Anal.* **1999**, *33*, 547–571. [CrossRef]
27. Levy, D.; Puppo, G.; Russo, G. A Fourth-Order Central WENO Scheme for Multidimensional Hyperbolic Systems of Conservation Laws. *SIAM J. Sci. Comput.* **2002**, *24*, 480–506. [CrossRef]
28. Balsara, D.S.; Garain, S.; Shu, C.-W. An efficient class of WENO schemes with adaptive order. *J. Comput. Phys.* **2016**, *326*, 780–804. [CrossRef]
29. Jiang, L.; Shan, H.; Liu, C. Weighted Compact Scheme for Shock Capturing. *Int. J. Comput. Fluid Dyn.* **2001**, *15*, 147–155. [CrossRef]
30. Fu, H.; Wang, Z.; Yan, Y.; Liu, C. Modified weighted compact scheme with global weights for shock capturing. *Comput. Fluids* **2014**, *96*, 165–176. [CrossRef]

31. Sod, G.A. A survey of several finite difference methods for systems of nonlinear hyperbolic conservation laws. *J. Comput. Phys.* **1978**, *27*, 1–31. [CrossRef]
32. Woodward, P.; Colella, P. The numerical simulation of two-dimensional fluid flow with strong shocks. *J. Comput. Phys.* **1984**, *54*, 115–173. [CrossRef]